



# PCCP

**Dissection of the multichannel reaction of acetylene with atomic oxygen: from global potential energy surface to rate coefficients and branching dynamics**

Journal:	<i>Physical Chemistry Chemical Physics</i>
Manuscript ID	CP-ART-11-2018-007084.R1
Article Type:	Paper
Date Submitted by the Author:	04-Dec-2018
Complete List of Authors:	Zuo, Junxiang; Nanjing University, School of Chemistry and Chemical Engineering Chen, Qixin; Nanjing University, School of Chemistry and Chemical Engineering Hu, Xixi; Nanjing University, School of Chemistry and Chemical Engineering Guo, Hua; University of New Mexico, Department of Chemistry Xie, Daiqian; Nanjing University, School of Chemistry and Chemical Engineering; University of Science and Technology of China, Synergetic Innovation Center of Quantum Information and Quantum Physics

SCHOLARONE™  
Manuscripts

Submitted to Phys. Chem. Chem. Phys., 16/11/2018, revised 4/12/2017

**Dissection of the multichannel reaction of acetylene with  
atomic oxygen: from global potential energy surface to rate  
coefficients and branching dynamics**

Junxiang Zuo,<sup>a</sup> Qixin Chen,<sup>a</sup> Xixi Hu,<sup>a,\*</sup> Hua Guo,<sup>b</sup> and Daiqian Xie<sup>a,c</sup>

*<sup>a</sup> Institute of Theoretical and Computational Chemistry, Key Laboratory of  
Mesoscopic Chemistry, School of Chemistry and Chemical Engineering, Nanjing  
University, Nanjing 210093, China*

*<sup>b</sup> Department of Chemistry and Chemical Biology, University of New Mexico,  
Albuquerque, New Mexico 87131, USA*

*<sup>c</sup> Synergetic Innovation Center of Quantum Information and Quantum Physics,  
University of Science and Technology of China, Hefei, Anhui 230026, China*

\*: corresponding author, [xxhu@nju.edu.cn](mailto:xxhu@nju.edu.cn) (X.H.)

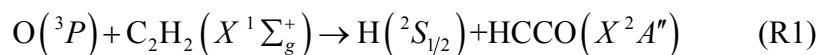
## Abstract

The  $O(^3P) + C_2H_2$  reaction is the first step in the significant acetylene oxidation. The accurate kinetic data and the understanding of the reaction dynamics is of great importance. To this end, a full-dimensional global potential energy surface (PES) for the ground triplet state of the  $O(^3P) + C_2H_2$  reaction is constructed based on approximately 85 000 *ab initio* points calculated at the level of explicitly correlated unrestricted coupled cluster single, double, and perturbative triple excitations with the explicitly correlated polarized valence triple zeta basis set (UCCSD(T)-F12b/VTZ-F12). The PES is fit using the permutation invariant polynomial-neural network (PIP-NN) approach with a total root mean square error of 0.21 kcal/mol. The key topographic features of the PES, including multiple potential wells and saddle points along different reaction pathways, are well represented by this fit PES. The kinetics and dynamics of the  $O(^3P) + C_2H_2$  reaction are investigated using the quasi-classical trajectory (QCT) method. The calculated rate coefficients are in good agreement with experimental data over a wide temperature range, especially when the temperature is lower than 1500 K. The product branch ratio has also been determined, which indicates the H + HCCO channel as the dominant reaction pathway at 298-3000 K, accounting for 80-90% of the overall rate coefficient, in agreement with experimental observations. The dynamics of the reaction is analyzed in detail.

## Introduction

A thorough understanding of complex chemical networks such as those for combustion requires a reliable theoretical description of both elementary kinetics and energy transfer steps. Despite unprecedented advances in recent years, the theoretical characterization of kinetics of elementary steps and product branching is still largely based on transition-state theory.<sup>1</sup> Such theory assumes that the kinetics is determined by reaction bottlenecks because energy randomization is complete. However, this assumption is not always met, especially in reactions involving a small number of atoms.<sup>2</sup> Hence, there is a need to examine the dynamics of such reactions and identify factors that may cause non-statistical behaviors.

Acetylene ( $C_2H_2$ ) is a major intermediate in most hydrocarbon flames. The oxidation of acetylene is of great relevance in combustion of hydrocarbons,<sup>3</sup> in hydrocarbon-rich planetary atmospheres,<sup>4</sup> as well as in interstellar media.<sup>5</sup> It is well established that the first step in acetylene oxidation is the reaction with the ground state oxygen atom  $O(^3P)$ , resulting in the following two primary product channels:



It was postulated<sup>6, 7</sup> that atomic oxygen first attacks a carbon atom of acetylene and forms triplet formylmethylene,  $OHCCH$ . This is followed by the decomposition of the  $OHCCH$  complex *via* either atomic hydrogen elimination to form  $HCCO$  or atomic hydrogen migration followed by a carbon-carbon bond fission leading to the  $CO$  and

CH<sub>2</sub> products.

Due to its importance in combustion, planetary atmospheres, and interstellar media, the O(<sup>3</sup>P) + C<sub>2</sub>H<sub>2</sub> reaction has in the past drawn considerable attention, both experimental<sup>8-24</sup> and theoretical.<sup>6, 7, 25-30</sup> A variety of experimental techniques has been used to measure kinetic and dynamic properties of the title reaction. Specifically, the rate coefficient for the reaction was determined over a wide temperature range and the results are consistent with each other.<sup>8-11, 14, 17, 18</sup> The value of the overall rate coefficient was recommended as  $1.94 \times 10^{-15} T^{1.40} \exp(-1110/T)$  cm<sup>3</sup> molecule<sup>-1</sup> s<sup>-1</sup> with the reliability of  $\Delta \log k = \pm 0.2$  over the range of 200-2000 K and  $\pm 0.3$  at 2500 K.<sup>31</sup> However, the product branching ratio (BR) is still controversial despite many studies over the years. Recent crossed molecular beam (CMB) experiments with soft electron ionization detection<sup>24</sup> have revealed that R1 is the dominant product channel with a BR of  $(79 \pm 5)\%$  at all collision energies studied.

Theoretical understanding of the reaction mechanism and dynamics relied on a detailed knowledge of the reaction pathways. To this end, *ab initio* calculations of the O(<sup>3</sup>P) + C<sub>2</sub>H<sub>2</sub> reaction have been performed by several groups to characterize stationary points along multiple reaction paths.<sup>7, 26, 27</sup> Nguyen *et al.*<sup>27</sup> reported the most detailed study of geometries and energies of stationary points on the lowest two triplet potential energy surfaces (PESs) using various quantum chemical methods. Their calculations, and those preceding ones, revealed that the reaction rate is largely determined by an entrance channel barrier as O attacks acetylene. Their calculated

thermal rate coefficient agreed well with experiment after they empirically lowered (by 0.5 kcal/mol) the *ab initio* entrance barrier obtained using the complete basis set-quadratic configuration interaction calculations based on atomic pair natural orbitals (CBS-QCI/APNO) level of theory. They have further predicted the branching ratio of the product and concluded that there are some non-statistical behaviors of the reaction. More recently, Garashchuk *et al.*<sup>29</sup> developed analytical triplet and singlet PESs for this system based on ~47 000 points at the restricted coupled cluster method with single, double, and perturbative triple excitations and correlation consistent aug-cc-pVTZ basis set (RCCSD(T)/AVTZ). The PESs were fit using the permutation invariant polynomial (PIP) method.<sup>32</sup> The root mean square deviation of the fit triplet PES is still significant (3.37 kcal/mol). Furthermore, the focus of that work was on the simulation of the hyperthermal collisional experiment of the Minton group for R1.<sup>23</sup> Neither thermal rate coefficient nor R1/R2 branching ratio was reported.

To obtain an accurate dynamical characterization of this important multichannel reaction, a more accurate global PES is needed for both R1 and R2. To achieve this goal, we report here a new full nine-dimensional PES for the ground triplet state of the OC<sub>2</sub>H<sub>2</sub> system based on ~85 000 high-level *ab initio* points, fit by the permutation invariant polynomial-neural network (PIP-NN) method.<sup>33, 34</sup> The use of the PIP-NN method results in a fitting error that is more than one order of magnitude smaller (0.21 kcal/mol) than before, even when the PES is extended beyond the R1 reaction channel. Using the new PIP-NN PES, we have calculated the thermal rate coefficients for R1, R2, and the overall reaction, using the quasi-classical trajectory (QCT) method. The

results are in excellent agreement with experiment. In addition, the QCT results are analyzed in detail to provide information on the main reaction pathways and residence times of key reaction intermediates. These mechanistic insights help to shed light on the unique product branching process.

## Methods

### *Ab initio* calculations

The *ab initio* calculations reported here employed an explicitly correlated (F12b) version of the unrestricted coupled cluster method with single, double, and perturbative triple excitations (UCCSD(T)) level of theory.<sup>33, 34</sup> The reference wave functions were based on the spin-restricted Hartree-Fock (RHF) method. For use with the explicitly correlated F12 method, the correlation-consistent polarized valence basis sets ranging in quality from double to quadruple zeta, denoted cc-pVnZ-F12 or VnZ-F12 ( $n = D, T, Q$ ),<sup>35</sup> were employed for determining the stationary points of the title reaction. As a compromise between accuracy and efficiency, the basis set of VTZ-F12 was chosen for *ab initio* calculations of points for constructing the global PES. All calculations were carried out using MOLPRO 2015.1.0.<sup>36</sup> Because we are mostly interested in a relative low-temperature range, only the lower  $^3A''$  state was considered. As discussed by Nguyen *et al.*,<sup>27</sup> the higher  $^3A'$  state is expected to contribute to the rate only at high temperatures, thanks to its higher entrance channel barrier.

### Construction of PES

The PES was fit using the PIP-NN method.<sup>37, 38</sup> The PIP-NN approach provides a simple, robust, and systematic framework to adapt the full permutation symmetry of the system, as demonstrated in fitting many PESs for both gas phase and gas–surface systems.<sup>39</sup> The essence of the method is to use low-order PIPs, rather than internuclear distances directly, as the input layer of the NN. The NN training is thus carried out within the PIP space, which strictly observes the permutation symmetry. For a system with five atoms, such as the OC<sub>2</sub>H<sub>2</sub> system, the PIP symmetry functions can be constructed in terms of symmetrized monomials<sup>40</sup> as following form,

$$\mathbf{X} = \hat{\mathbf{S}} \prod_{i < j}^5 p_{ij}^{l_{ij}}, \quad (2)$$

where  $p_{ij} = \exp(-\alpha r_{ij})$  represent Morse-like variables with  $\alpha = 0.5 \text{ bohr}^{-1}$  and  $l_{ij}$  is the order of each monomial.  $\hat{\mathbf{S}}$  is the symmetrization operator, which consists of all possible nuclear permutation operations in the system. With  $\mathbf{X} = \{X_i\}$  being the input, a standard feed-forward NN with two hidden layers was constructed. The value of the  $k^{\text{th}}$  neuron of the  $i^{\text{th}}$  hidden layer can be written as

$$y_k^i = f^i \left( b_k^i + \sum_{j=1}^{N_{i-1}} (w_{jk}^i \cdot y_j^{i-1}) \right), \quad 1 \leq i \leq 2, \quad (3)$$

in which  $N_{i-1}$  is the number of neurons in the  $(i-1)^{\text{th}}$  layer, which equals the number of PIPs in the input layer when  $i=1$ .  $w_{jk}^i$  is the weight connecting the  $j^{\text{th}}$  neuron of  $(i-1)^{\text{th}}$  layer and  $k^{\text{th}}$  neuron of  $i^{\text{th}}$  layer,  $b_k^i$  is the bias on the  $k^{\text{th}}$  neuron of the  $i^{\text{th}}$  layer. The transfer function  $f^i$  is usually in the form of a hyperbolic function for the neurons in the hidden layers and a linear function for those

in the input and output layers.

The NNs were trained utilizing the Levenberg-Marquardt algorithm<sup>41</sup> and the ‘early stopping’ method<sup>42</sup> was used to avoid overfitting. To measure the performance, the root mean square error (RMSE), defined as

$$\text{RMSE} = \sqrt{\sum_{i=1}^{N_{\text{data}}} (E_i^{\text{PES}} - E_i^{\text{ab initio}})^2 / N_{\text{data}}}, \quad (4)$$

was used. Here,  $E_i^{\text{PES}}$  and  $E_i^{\text{ab initio}}$  are the fit energy and *ab initio* energy of the  $i^{\text{th}}$  point, respectively.

We obtained the first set of *ab initio* points (about 8 000 configurations) by carefully varying the bond lengths, bond angles, and dihedral angles near the stationary points reported by Nguyen *et al.*<sup>27</sup> With these initial points, a primitive PES was first constructed. Additional *ab initio* points were generated using classical trajectories on this primitive PES. Points with energies higher than 115.30 kcal/mol relative to the minimum of the PES were discarded. Besides, a criteria based on the Euclidean distance defined between two configurations,  $\chi = \sqrt{\sum_{i=1}^{10} |\mathbf{r}_i - \mathbf{r}'_i|^2}$ , was employed to remove points that are too close to those in the training set ( $\chi \leq 0.15$  Å). This procedure was repeated until convergence. Finally, a total of 84 598 *ab initio* points was calculated at the level of UCCSD(T)-F12b/VTZ-F12 and used to construct the PES employing the PIP-NN method.

In the PIP-NN fitting, all 101 PIPs up to the third order ( $l \leq 3$ ) were used in the

input layer and a NN architecture with two hidden layers of 50 and 80 neurons was selected, resulting in 9261 parameters. To avoid overfitting, the database was randomly divided into the training (90%), validating (5%), and testing (5%) sets. The three best PIP-NN fits were chosen from 100 different training calculations. To further reduce the random errors, the final PES is the average of these three best PIP-NN fits.

### QCT calculations

In this work, QCT calculations for the  $O(^3P) + C_2H_2$  reaction were performed using the VENUS code.<sup>43,44</sup> In QCT calculations, the trajectories were propagated on the PES by solving Newton's equation numerically. At each temperature, batches ( $10^5$ - $10^6$ ) of trajectories were calculated. The initial ro-vibrational energy of  $C_2H_2$  and translational energy between  $O(^3P)$  and  $C_2H_2$  were sampled in terms of the Boltzmann distribution at each temperature. The maximal impact parameter  $b_{\max}$  was determined using small batches of trajectories with trial values. The trajectories were initiated with a 10 Å separation between reactants of  $O(^3P)$  and  $C_2H_2$  and terminated when products of  $H + HCCO$  (or  $CO + CH_2$ ) reached a separation of 8.0 Å or reactants for nonreactive trajectories reached a separation of 10.5 Å. The propagation time step was selected to be 0.1 fs which conserved the energies better than 0.01 kcal/mol for most trajectories. The trajectories were halted if the propagation time is exceptionally long (10.0 ps). A few trajectories which failed to converge energy to chosen criteria or were nonreactive after 10.0 ps were discarded. To mitigate ZPE

leakage, the so-called “passive” method<sup>45</sup> was applied to both two product channels.

The trajectories violating ZPE constraints were removed.

The thermal rate coefficient for the  $O(^3P) + C_2H_2$  reaction at temperature ranging from 298 to 3000 K was calculated as follows:

$$k(T) = g_e \left( \frac{8k_B T}{\pi\mu} \right)^{1/2} \pi b_{\max}^2 \frac{N_r}{N_{\text{total}}} \quad (5)$$

In which  $k_B$  is the Boltzmann constant and  $\mu$  is the reduced mass of the two reactants species, namely,  $\mu = m_O m_{C_2H_2} / (m_O + m_{C_2H_2})$ .  $N_r$  and  $N_{\text{total}}$  are numbers of reactive and total trajectories. The electronic degeneracy factor for the spin-orbit states of  $O(^3P)$ ,  $g_e = 3 / (5 + 3 \exp(-158.5 \text{cm}^{-1} / k_B T) + \exp(-226.5 \text{cm}^{-1} / k_B T))$ , was used. The statistic error is given by  $\Delta = [(N_{\text{total}} - N_r) / (N_{\text{total}} N_r)]^{1/2}$ .

## Results

### Features of the PES

First, we examine the influence of the basis set on the energetics. In Table 1, UCCSD(T)-F12 energies of the stationary points along the reaction pathways are compared for different  $VnZ$ -F12 basis sets. It is clear that the results of VTZ-F12 and VQZ-F12 are quite close, consistent with the fast convergence of the F12 method with respect to the basis size.<sup>33, 34</sup> Hence, the former was used in generating the PES points.

The PES has complex topography. Fig. 1 shows geometries of all stationary points and their energies relative to the reactant asymptote. The reaction pathways consist of

seven transition states (TS1-TS7) and four reaction complexes (Int1-Int4). The  $O(^3P) + C_2H_2$  reaction proceeds initially *via* a shallow pre-reaction well (Int1) and the rate-limiting barrier (TS1). The classical barrier height of TS1 computed at the UCCSD(T)-F12/VTZ-F12 level is 3.57 kcal/mol, which is close to the CBS-QCI/APNO value (3.5 kcal/mol) reported by Nguyen *et al.*<sup>27</sup> TS1 is connected *via* the intrinsic reaction coordinate with Int2, which is the *trans* form (with respect to the two hydrogens) of the formylmethylene intermediate.

Starting from Int2, there are several possible microscopic reaction pathways on the PES. The first one proceeds *via* a very low isomerization barrier (TS2) to the *cis* form of the formylmethylene intermediate (Int3). The barrier height of 6.75 kcal/mol is much lower than the energy release from TS1. As a result, facile isomerization is expected. The *cis*-isomer (Int3) can dissociate directly to P1 (HCCO + H) *via* a barrier of 39.73 kcal/mol (TS5) or convert to Int4 *via* a much higher (51.68 kcal/mol) barrier (TS6) through 1,2-hydrogen shift. Int4 eventually dissociates into P2 (CO + CH<sub>2</sub>) *via* TS7 with a low barrier of 29.92 kcal/mol. The second path starting from Int2 undergoes 1,2-hydrogen shift to a ketene (Int4), also through a barrier (TS4) of 45.38 kcal/mol. In the third path, Int2 dissociates directly to P1 *via* H elimination, though TS3 with a barrier of 48.23 kcal/mol. We note here in passing that the energetics discussed here does not necessarily provide the correct picture of the reaction mechanism, due to the neglect of dynamics.

The complex topography of the PES makes the fitting very difficult, but the

PIP-NN approach is demonstrated again to be sufficiently flexible for representing the multichannel PES. The total RMSEs and the maximum deviations of the three best PIP-NN fits are 0.26/13.41, 0.26/11.67, and 0.26/21.90 kcal/mol, respectively. The total RMSE of the final PES is 0.21 kcal/mol with a maximum deviation 12.66 kcal/mol. The distribution of *ab initio* points as a function of the potential energy is shown in Fig. 2(a). In addition, the fitting errors of all *ab initio* data and their distribution are presented in Figs. 2(b) and 2(c). It is clear that the fitting is quite faithful. Indeed, the *ab initio* energies of the stationary points on the fit PES listed in Fig. 1 are well reproduced by the PES, with a deviation between the two less than 0.16 kcal/mol. The optimized stationary point geometries and harmonic vibrational frequencies on the PES are also in excellent agreement with the *ab initio* counterparts, as shown in Supporting Information (SI), Tables S1 and S2.

The entrance channel of the PES along two reactive coordinates, namely,  $R_{OC}$  and  $\theta_{OCC}$ , is displayed in Fig. 3, with all other coordinates constrained at the transition state (TS1) geometry. It is clear from the contours that the reaction has a reactant-like barrier (TS1, indicated by a red star) in the entrance channel. The transition state TS1, which is the key kinetic reaction bottleneck, features a planar geometry with 3.57 kcal/mol above the reactant asymptote. The calculated reaction barrier of TS1 is only slightly larger than experimentally derived Arrhenius activation energy,<sup>14, 17, 18, 31, 46</sup> namely 3-3.5 kcal/mol. Notably, a shallow complex well (Int1, -1.13 kcal/mol relative to reactant asymptote) is found for the first time for this reaction and this entrance channel well can be identified easily in the figure. The Int1 complex has a nearly

T-shape geometry in which the forming O-C bond distance is 2.96 Å, the OCC angles are both 78.3°, and the HCC angles are both 179.9°.

As shown in Table S2, the reaction exothermicity of the H + HCCO channel is -19.64 kcal/mol with the zero point energy (ZPE) correction, which is in excellent agreement with the experimental value ( $D_0 = -19.85 \pm 0.51$ ) kcal/mol.<sup>47, 48</sup> For R2, the reaction exothermicity of -48.30 kcal/mol is about 1.0 kcal/mol (2%) larger than the experimental value, ( $D_0 = -47.30 \pm 0.23$ ) kcal/mol.<sup>48</sup>

### Rate coefficients and branching ratios

Based on the new PIP-NN PES, the rate coefficients for both H + HCCO and CO + CH<sub>2</sub> channels of the O(<sup>3</sup>P) + C<sub>2</sub>H<sub>2</sub> reaction on the lowest triplet state PES were calculated utilizing the QCT method. Nonadiabatic transitions to the other triplet state or to singlet state are not considered in this work.  $6.7 \times 10^5$  (298 K),  $1.5 \times 10^5$  (500 K), and  $1.0 \times 10^5$  (>500 K) trajectories were calculated at temperatures of 298, 500, 1000, 1500, 2000, 2500 and 3000 K and the statistical error of trajectories were 0.071, 0.042, 0.017, 0.012, 0.009, 0.008, and 0.007, respectively. The majority of trajectories conserved energy within the criterion of  $10^{-4}$  kcal/mol and it implied that the PES is smooth and free of discontinuity. The results of QCT calculations for the O(<sup>3</sup>P) + C<sub>2</sub>H<sub>2</sub> reaction rate coefficients obtained on the new PIP-NN PES are summarized in Table 2. For comparison, previous rate coefficients<sup>27</sup> derived from transition state theory (TST) are also listed in the table. The calculated QCT rate coefficients for the title reaction over the temperature 298-3000 K are compared in Fig. 4 with the

experimental<sup>8-11, 14, 17, 18, 31</sup> and previous theoretical<sup>27</sup> results. From the table and figure, it is apparent that the QCT rate coefficient exhibits the Arrhenius type temperature dependence and agrees well with the experimental values over a wide temperature range from 298 to 1500 K. At 298 K, the calculated rate coefficient value of  $1.30 \times 10^{-13} \text{ cm}^3 \text{ molecule}^{-1} \text{ s}^{-1}$  is almost identical with the experimental value of  $1.37 \times 10^{-13} \text{ cm}^3 \text{ molecule}^{-1} \text{ s}^{-1}$  recommended by Baulch *et al.*<sup>31</sup>

Interestingly, both the QCT and experimental rate coefficients deviate from the Arrhenius behavior above 1500 K. However, our QCT rate coefficients underestimate the experimental values<sup>11, 18</sup> and the deviation increases with the temperature. The theory-experiment deviation is almost certainly due to the neglect of the excited  $^3A'$  state. Nguyen *et al.*<sup>27</sup> have pointed out the reaction pathway on the electronically excited  $^3A'$  state resulting excited products  $\text{H}(^2S) + \text{HCCO}(^9\%A')$  becomes important at high temperatures and may contribute as much as 30% to the overall rate coefficients at 2000 K. From Table 2 and Fig. 4, it is clear that QCT rate coefficients are quite close to TST values at low temperatures (within 6.9% at 298 K), but the deviation increases with the temperature (TST rate coefficient is 2.8 times larger than QCT one at 2000 K). This is because the TST results include the contribution from the electronically excited  $^3A'$  state.

The product branching fractions in the whole range of calculation temperature are also listed in Table 2. It is clear that the  $\text{H} + \text{HCCO}$  channel is the dominant reaction pathway and accounts for 80-90% of the total product yield in the  $\text{O}(^3P) + \text{C}_2\text{H}_2$

reaction. In addition, the branching fractions are relatively insensitive to temperature. These results are consistent with the earlier rate measurements<sup>18, 19</sup> and the most recent molecular beam experiments,  $(79 \pm 5) \%$  for R1, by Leonori *et al.*<sup>24</sup> at several collision energies. The good agreement between QCT rate coefficients and branching ratio implies that the impact of tunneling is limited in titled reactions. Nguyen *et al.*<sup>27</sup> has also pointed out that tunneling only increase the absolute yield of P2 product channel by 0.6% at 298 K. It is not surprising, since the crossing of the rate limiting barrier involves mostly the attack of C by O, no H motion is significantly involved.

## Discussion

To gain further understanding of the reaction dynamics, particularly the product branching mechanism, we have analyzed the reaction flux through different reaction pathways. Nguyen *et al.*<sup>27</sup> have argued that the discrepancy between the calculated and measured branching ratios might be due to the lack of equilibrium between the two key reaction intermediates, Int2 or Int3.<sup>27</sup> To test this hypothesis, we have investigated their formation and depletion as well as residence times, in which the intermediates are identified by geometric parameters defined in Table 3.

The two upper panels in Fig. 5 present the percentages of reactive trajectories that first reach Int2 (red bar) and Int3 (blue bar) after overcoming TS1 and eventually end up in the H + HCCO (Fig. 5(a)) and the CO + CH<sub>2</sub> (Fig. 5(b)) product channels, respectively. (Note that there might be multiple conversions between the two isomers before eventually reaching the product channels.) It is clear from these results that the

initial attack of acetylene by O mostly results first in the formation of Int2, irrespective of the final product channels. This is particularly true at low temperatures. The preference for the initial formation of Int2 is easy to understand since the intrinsic reaction coordinate of TS1 leads directly to Int2, while the formation of Int3 requires energy flow from the reaction coordinate to the torsional degree of freedom. The latter becomes possible at higher temperatures because of the initial energy in the torsional mode.

The final branching dynamics are revealed by the two lower panels of Fig. 5, which show the last product forming step of the reaction. In Fig. 5(c), the dominant P1 channel is produced mostly from Int3 *via* TS5 (blue bar), with a minor contribution from Int2 through TS3 (red bar). This is likely due to the lower barrier at TS5. On the other hand, as shown in Fig. 5(d), the minor P2 channel is mostly from Int2 to Int4 through TS4 (red bar), but also from Int3 to Int4 *via* TS6 (blue bar) as a minor channel. This preference is presumably due to the higher barrier at TS6.

Between the initial formation of the Int2/Int3 intermediates and the final exit to the product channels, there is facile isomerization between the two intermediates (data not shown), thanks to the low isomerization barrier. In Fig. 6, the ratio between the total residence times of Int2 and Int3 is plotted as a function of the total reaction time for all reactive trajectories at several temperatures. Here the total reaction time of a trajectory is defined as the length of the propagation. This figure contains a wealth of information. First, it shows that there are both fast and slow reactions, and the former becomes dominant as temperature increases. This fast and direct channel typically

takes about 50-200 fs and involves only a few conversions between the Int2 and Int3 isomers, while the slow one ( $t > 300$  fs), which can be categorized as a complex-forming mechanism, undergoes many isomerization (data not shown). Second, in the slow channel, all trajectories have roughly the same ratio, and it is slightly above 1.0. This is consistent with a microcanonical equilibrium between the two isomers as Int3 has a slightly higher energy, thus less population. However, in the fast channel, the ratio is quite scattered, signaling that the system has not reached an equilibrium. This non-statistical nature of the fast channel is consistent with the conclusion of Nguyen *et al.*<sup>27</sup> However, no significant difference of the branching ratio was found between the fast and slow channels, as shown by the data in Table 4.

These analyses thus paint a clear picture of the reaction dynamics and product branching. After the initial surmount of a common transition state (TS1), the system typically settles in the Int2 intermediate. Facile conversions between the Int2 and Int3 conformers ensure subsequently. The eventually formation of the two product channels are dominated by the passage of TS5 from Int3 to P1 and TS4 from Int2 to P2.

## Conclusions

To summarize, we have constructed a full-dimensional global ground triplet state PES for the  $O(^3P) + C_2H_2$  reaction. The PES is constructed by fitting roughly 85 000 *ab initio* points calculated at the UCCSD(T)-F12b/VTZ-F12 level, using the PIP-NN method. The stationary points, including intermediate wells and transition states, are

well characterized by the new PES, which sheds light on both the H + HCCO and CO + CH<sub>2</sub> reaction pathways. Extensive QCT calculations have been performed on the PIP-NN PES, and rate coefficients of O(<sup>3</sup>P) + C<sub>2</sub>H<sub>2</sub> reaction over 298-3000 K were obtained and compared with the available experimental values. Good agreement between theoretical and experimental results has been achieved for both rate constants and product branching ratio, especially when the temperature is lower than 1500 K. The good agreement provides supporting evidence for the accuracy of the fit PES. It is expected that this new accurate PES will provide a reliable platform for the kinetic and dynamical studies of this reaction in the future.

To gain insight into the reaction mechanism, we have also analyzed the reaction flux to provide insights into the reaction mechanisms and dynamics. It is shown that Int2 is preferentially produced after overcoming the rate-limiting barrier in the entrance channel (TS1). It is followed by facile isomerization between Int2 and Int3. Finally, the dominate H + HCCO product is mostly formed from Int3 *via* TS5, while the minor CO + CH<sub>2</sub> channel from Int2 *via* TS4. Furthermore, the two intermediates are found to achieve a microcanonical equilibrium for the long-lived complex-forming mechanism, but such an equilibrium is not established in the direct mechanism. Nonetheless, the branching ratio is not significantly affected by the lack of equilibration in the latter. These details help to shed light on the dynamics of this multi-channel reaction. Comparison with transition-state theory suggests that even when the reaction is not completely statistical the transition-state theory still provides reasonably satisfactory results.

## **Conflicts of interest**

There are no conflicts to declare.

## **Acknowledgements**

X.H. acknowledges financial support from National Natural Science Foundation of China (Grant Nos. 91641104). D.X. thanks financial support from National Natural Science Foundation of China (Grant Nos. 21590802 and 21733006). H.G. is supported by US Department of Energy (Grant No. DE-SC0015997). We sincerely thank Prof. Jun Li for many useful discussions on the QCT calculations.

## References

1. S. J. Klippenstein, *Proc. Combust. Inst.*, 2017, **36**, 77-111.
2. U. Lourderaj and W. L. Hase, *J. Phys. Chem. A*, 2009, **113**, 2236-2253.
3. D. J. Hucknal, *Chemistry of Hydrocarbon Combustion*, Chapman Hall, New York, 1985.
4. M. Dobrijevic, E. Hébrard, J. C. Loison and K. M. Hickson, *Icarus*, 2014, **228**, 324-346.
5. A. Occhiogrosso, S. Viti and N. Balucani, *Mon. Not. R. Astron. Soc.*, 2013, **432**, 3423-3430.
6. L. B. Harding, *J. Phys. Chem.*, 1981, **85**, 10-11.
7. L. B. Harding and A. F. Wagner, *J. Phys. Chem.*, 1986, **90**, 2974-2987.
8. K. Hoyeremann, H. G. Wagner and J. Wolfrum, *Z. Phys. Chem.*, 1969, **63**, 193-196.
9. G. S. James and G. P. Glass, *J. Chem. Phys.*, 1969, **50**, 2268-2269.
10. A. A. Westenbeg and N. deHaas, *J. Phys. Chem.*, 1969, **73**, 1181-1186.
11. R. Löhr and P. Roth, *Ber. Bunsenges. Phys. Chem.*, 1981, **85**, 153-158.
12. A. R. Clemo, G. L. Duncan and R. Grice, *J. Chem. Soc., Faraday Trans. 2*, 1982, **78**, 1231-1238.
13. J. Peeters, M. Schaekers and C. Vinckier, *J. Phys. Chem.*, 1986, **90**, 6552-6557.
14. K. Mahmud and A. Fontijn, *J. Phys. Chem.*, 1987, **91**, 1918-1921.
15. J. Peeters, S. Vanhaelemeersch, J. Van Hoeymissen, R. Borms and D. Vermeylen, *J. Phys. Chem.*, 1989, **93**, 3892-3894.
16. A. M. Schmoltner, P. M. Chu and Y. T. Lee, *J. Chem. Phys.*, 1989, **91**, 5365-5373.
17. B. Bohn and F. Stuhl, *J. Phys. Chem.*, 1990, **94**, 8010-8011.
18. J. V. Michael and A. F. Wagner, *J. Phys. Chem.*, 1990, **94**, 2453-2464.
19. W. Boullart and J. Peeters, *J. Phys. Chem.*, 1992, **96**, 9810-9816.
20. X. Huang, G. Xing and R. Bersohn, *J. Chem. Phys.*, 1994, **101**, 5818-5823.
21. G. Capozza, E. Segoloni, F. Leonori, G. G. Volpi and P. Casavecchia, *J. Chem. Phys.*, 2004, **120**, 4557-4560.
22. V. Chikan and S. R. Leone, *J. Phys. Chem. A*, 2005, **109**, 2525-2533.
23. S. A. Lahankar, J. Zhang, S. Garashchuk, G. C. Schatz and T. K. Minton, *J. Phys. Chem. Lett.*, 2013, **4**, 1315-1321.
24. F. Leonori, N. Balucani, G. Capozza, E. Segoloni, G. G. Volpi and P. Casavecchia, *Phys. Chem. Chem. Phys.*, 2014, **16**, 10008-10022.
25. D. R. Yarkony, *J. Phys. Chem. A*, 1998, **102**, 5305-5311.
26. Y. Girard and P. Chaquin, *J. Phys. Chem. A*, 2003, **107**, 10462-10470.
27. T. L. Nguyen, L. Vereecken and J. Peeters, *J. Phys. Chem. A*, 2006, **110**, 6696-6706.
28. K. Rajak and B. Maiti, *J. Chem. Phys.*, 2010, **133**, 011101.
29. S. Garashchuk, V. A. Rassolov and B. J. Braams, *Chem. Phys. Lett.*, 2013, **588**, 22-26.
30. K. Rajak and B. Maiti, *J. Chem. Phys.*, 2014, **140**, 044314.
31. D. L. Baulch, C. T. Bowman, C. J. Cobos, R. A. Cox, T. Just, J. A. Kerr, M. J. Pilling, D. Stocker, J. Troe, W. Tsang, R. W. Walker and J. Warnatz, *J. Phys. Chem. Ref. Data*, 2005, **34**, 757-1397.
32. B. J. Braams and J. M. Bowman, *Int. Rev. Phys. Chem.*, 2009, **28**, 577-606.
33. T. B. Adler, G. Knizia and H. J. Werner, *J. Chem. Phys.*, 2007, **127**, 221106.
34. G. Knizia, T. B. Adler and H. J. Werner, *J. Chem. Phys.*, 2009, **130**, 054104.

35. K. A. Peterson, T. B. Adler and H. J. Werner, *J. Chem. Phys.*, 2008, **128**, 084102.
36. H. J. Werner, P. J. Knowles, G. Knizia, F. R. Manby and M. Schütz, *Wiley Interdiscip. Rev.: Comput. Mol. Sci.*, 2012, **2**, 242-253.
37. B. Jiang and H. Guo, *J. Chem. Phys.*, 2013, **139**, 054112.
38. J. Li, B. Jiang and H. Guo, *J. Chem. Phys.*, 2013, **139**, 204103.
39. B. Jiang, J. Li and H. Guo, *Int. Rev. Phys. Chem.*, 2016, **35**, 479-506.
40. Z. Xie and J. M. Bowman, *J. Chem. Theory Comput.*, 2010, **6**, 26-34.
41. M. T. Hagan and M. B. Menhaj, *IEEE Trans. Neural Netw.*, 1994, **5**, 989-993.
42. L. M. Raff, R. Komanduri, M. Hagan and S. T. S. Bukkapatnam, *Neural Networks in Chemical Reaction Dynamics*, Oxford University Press, Oxford, 2012.
43. X. Hu, W. L. Hase and T. Pirraglia, *J. Comput. Chem.*, 1991, **12**, 1014-1024.
44. W. L. Hase, R. J. Duchovic, X. Hu, A. Komornicki, K. F. Lim, D. H. Lu, G. H. Peslherbe, K. N. Swamy, S. R. R. Vande Linde and A. Varandas, *J. Quantum Chem. Program Exch. Bull.*, 1996, **16**, 671.
45. Y. Guo, D. L. Thompson and T. D. Sewell, *J. Chem. Phys.*, 1996, **104**, 576-582.
46. P. M. Sheaffer and P. F. Zittel, *J. Phys. Chem. A*, 2000, **104**, 10194-10201.
47. NIST web page: <https://cccbdb.nist.gov/exp2x.asp>.
48. M. W. Chase, Davies, C.A., Downey, J.R., Frurip, D.R., McDonald, R.A. and Syverud, A.N., *J. Phys. Chem. Ref. Data*, 1985, **14**.

**Table 1** Comparison of UCCSD(T)-F12b energies of stationary points for the  $O(^3P) + C_2H_2$  reaction using different  $VnZ-F12(n=D, T, Q)$  basis sets. Energies are in unit of kcal/mol with respect to the  $O(^3P) + C_2H_2$  asymptote. The abbreviated labels of the stationary points can be found in Figure 1.

Basis set	R	P1	P2	Int1	Int2	Int3	Int4
VDZ-F12	0.00	-14.13	-45.95	-1.01	-52.97	-51.44	-71.93
VTZ-F12	0.00	-14.70	-45.60	-1.07	-53.46	-51.96	-72.58
VQZ-F12	0.00	-14.93	-45.67	-1.06	-53.69	-52.21	-72.83
Basis set	TS1	TS2	TS3	TS4	TS5	TS6	TS7
VDZ-F12	3.68	-46.20	-4.48	-7.07	-11.60	0.35	-42.70
VTZ-F12	3.55	-46.66	-5.19	-7.90	-12.25	-0.13	-42.65
VQZ-F12	3.48	-46.90	-5.44	-8.17	-12.47	-0.35	-42.79

**Table 2** Rate coefficients ( $\text{cm}^3 \text{ molecule}^{-1} \text{ s}^{-1}$ ) and branching ratios for the  $\text{O}(^3P) + \text{C}_2\text{H}_2$  reaction obtained from QCT calculations.  $k_{\text{QCT}}$  is total rate coefficients.  $k_1$  and  $k_2$  are rate coefficients for the  $\text{H} + \text{HCCO}$  and  $\text{CO} + \text{CH}_2$  channels, respectively. For comparison, previous rate coefficients<sup>27</sup> derived from transition state theory,  $k_{\text{TST}}$ , are also listed. Note that the TST rate coefficients include contribution of both electronic states.

$T / \text{K}$	298	500	1000	1500	2000	2500	3000
$k_1$	$1.07 \times 10^{-13}$	$1.01 \times 10^{-12}$	$5.61 \times 10^{-12}$	$1.10 \times 10^{-11}$	$1.64 \times 10^{-11}$	$2.15 \times 10^{-11}$	$2.59 \times 10^{-11}$
$k_2$	$2.33 \times 10^{-14}$	$1.25 \times 10^{-13}$	$9.09 \times 10^{-13}$	$2.05 \times 10^{-12}$	$3.35 \times 10^{-12}$	$4.82 \times 10^{-12}$	$6.33 \times 10^{-12}$
$k_{\text{QCT}}$	$1.30 \times 10^{-13}$	$1.14 \times 10^{-12}$	$6.51 \times 10^{-12}$	$1.30 \times 10^{-11}$	$1.97 \times 10^{-11}$	$2.63 \times 10^{-11}$	$3.23 \times 10^{-11}$
$k_{\text{TST}}^{27}$	$1.39 \times 10^{-13}$	$1.45 \times 10^{-12}$	$1.22 \times 10^{-11}$	$3.11 \times 10^{-11}$	$5.54 \times 10^{-11}$	-	-
$k_1/k_{\text{QCT}}$ (%)	82.14	88.99	86.05	84.31	82.99	81.65	80.37
$k_2/k_{\text{QCT}}$ (%)	17.86	11.01	13.95	15.69	17.01	18.35	19.63

**Table 3** Geometry parameters used to identify Int2 and Int3. Distances and angles are in units of Å and °, respectively.

	Int2		Int3	
	Equilibrium geometry	value range	Equilibrium geometry	value range
$r_{\text{OC}_1}$	1.232	0.932~1.532	1.224	1.024~1.424
$r_{\text{C}_1\text{C}_2}$	1.425	1.125~1.725	1.426	1.276~1.576
$r_{\text{C}_1\text{H}_1}$	1.097	0.797~1.397	1.108	0.908~1.308
$r_{\text{C}_2\text{H}_2}$	1.082	0.782~1.682	1.081	0.881~1.281
$\theta_{\text{OC}_1\text{C}_2}$	119.9	90.0~165.0	125.3	90.0~165.0
$\theta_{\text{H}_1\text{C}_1\text{C}_2}$	118.9	90.0~165.0	114.3	90.0~165.0
$\theta_{\text{C}_1\text{C}_2\text{H}_2}$	129.3	90.0~165.0	131.5	90.0~165.0
$\varphi_{\text{H}_1\text{C}_1\text{C}_2\text{O}}$	180.0	120.0~240.0	180.0	120.0~240.0
$\varphi_{\text{OC}_1\text{C}_2\text{H}_2}$	0	-60.0~60.0	180.0	120.0~240.0

**Table 4** The number of trajectories belong to P1 or P2 with total lifetime below 300 fs or above 400 fs at different temperatures. (P: P1+P2)

T / K	N ( $t_{\text{total}} < 300$ fs)				N ( $t_{\text{total}} > 400$ fs)				Statistica l error
	P1	P2	P1/P	P2/P	P1	P2	P1/P	P2/P	
298	69	12	85.2%	14.8%	75	18	80.7%	19.4%	7.1%
500	259	30	89.6%	10.4%	178	20	89.9%	10.1%	4.2%
1000	1798	293	86.0%	14.0%	797	140	85.1%	14.9%	1.7%
1500	4099	791	83.8%	16.2%	1137	185	86.0%	14.0%	1.2%
2000	7065	1524	82.3%	17.7%	1216	182	87.0%	13.0%	0.9%
2500	9434	2192	81.2%	18.9%	970	152	86.4%	13.6%	0.8%
3000	1110 5	2752	80.1%	19.9%	745	159	82.4%	17.6%	0.7%



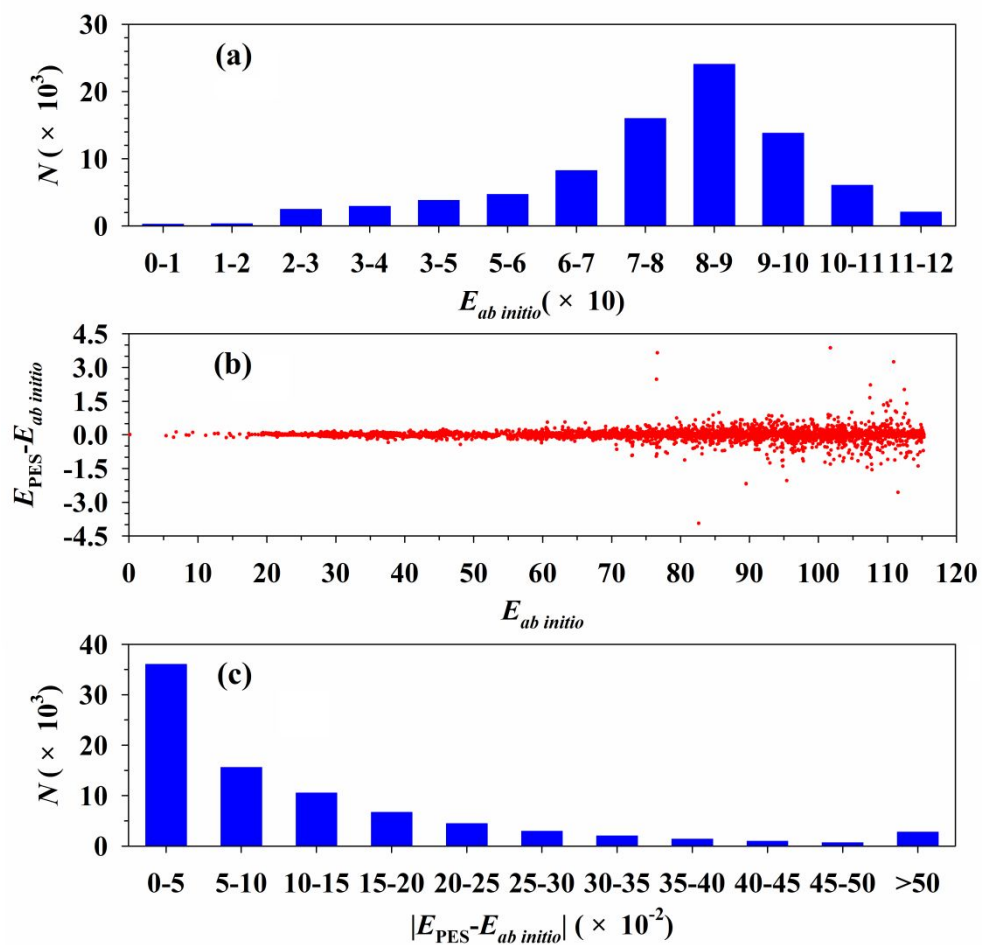


**Fig. 2** (a) Distribution of  $ab\ initio$  points for the PIP-NN PES. (b) Fitting errors as a function of the  $ab\ initio$  energy. (c) Distribution of the fitting errors for the selected points. The values of the potential energy are relative to the global minimum, Int4. All energies are in unit of kcal/mol.

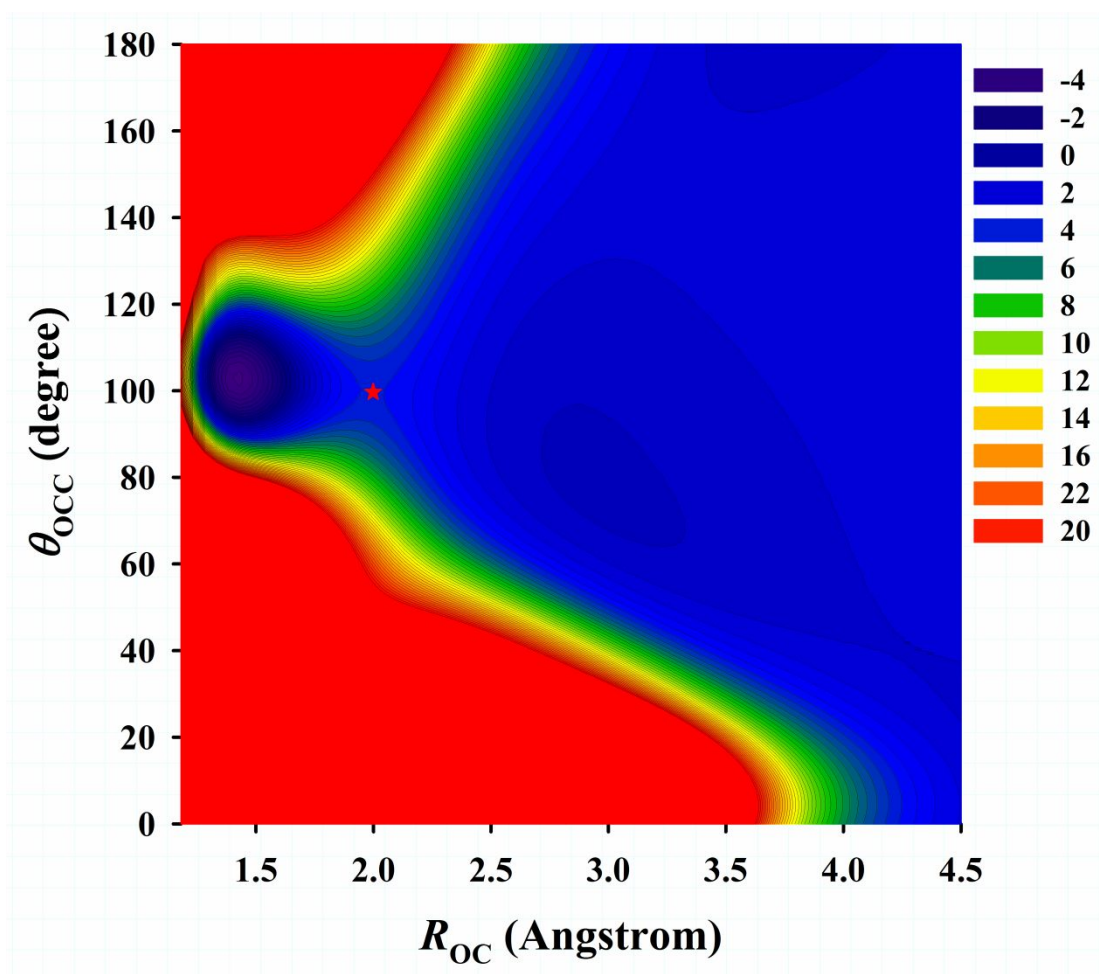


**Fig. 3** Contour plots of the  $\text{OC}_2\text{H}_2$  ( $^3A''$ ) PES as a function of two reactive coordinates,  $R_{\text{OC}}$  and  $\theta_{\text{OCC}}$ , with all other coordinates constrained at the transition state TS1. The energies are in kcal/mol relative to the  $\text{O}(^3P) + \text{C}_2\text{H}_2$  asymptote with an interval of 0.5 kcal/mol.

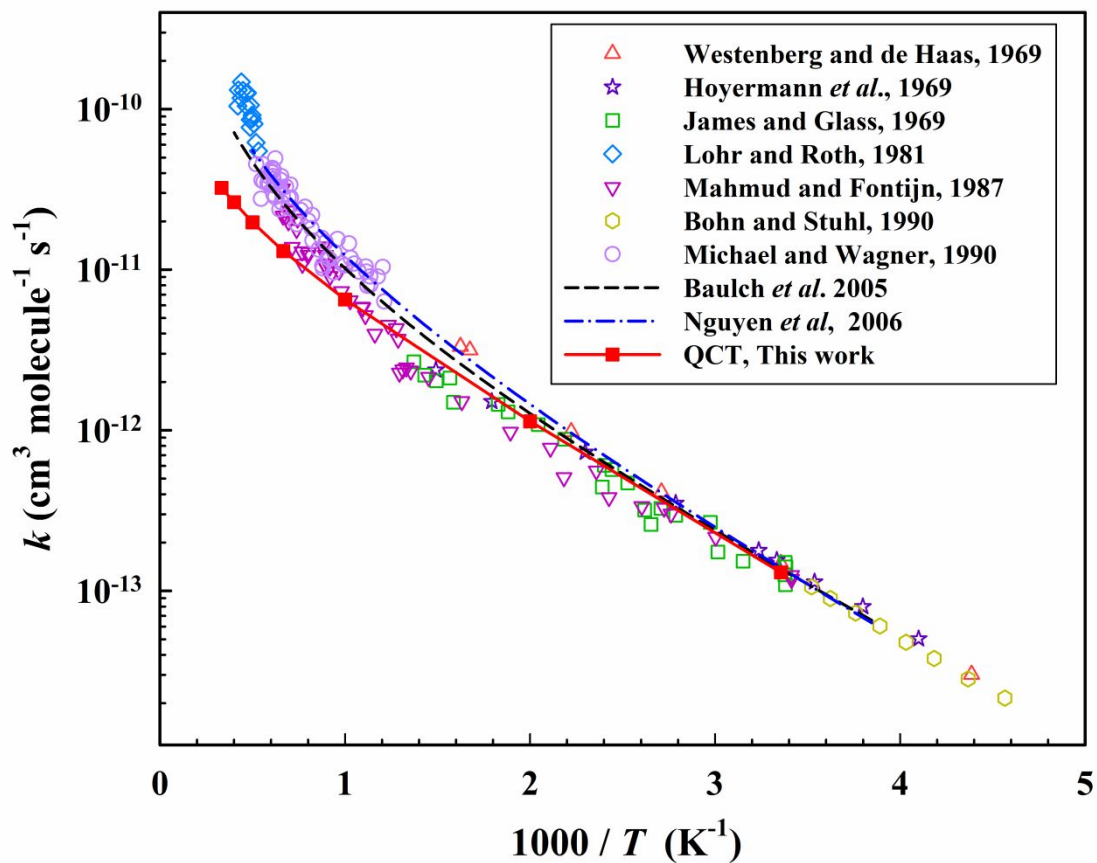


**Fig. 4** Arrhenius plot for the  $\text{O}(^3P) + \text{C}_2\text{H}_2$  reaction rate coefficient compared with previous theoretical<sup>27</sup> and experimental<sup>8-11, 14, 17, 18, 31</sup> results.

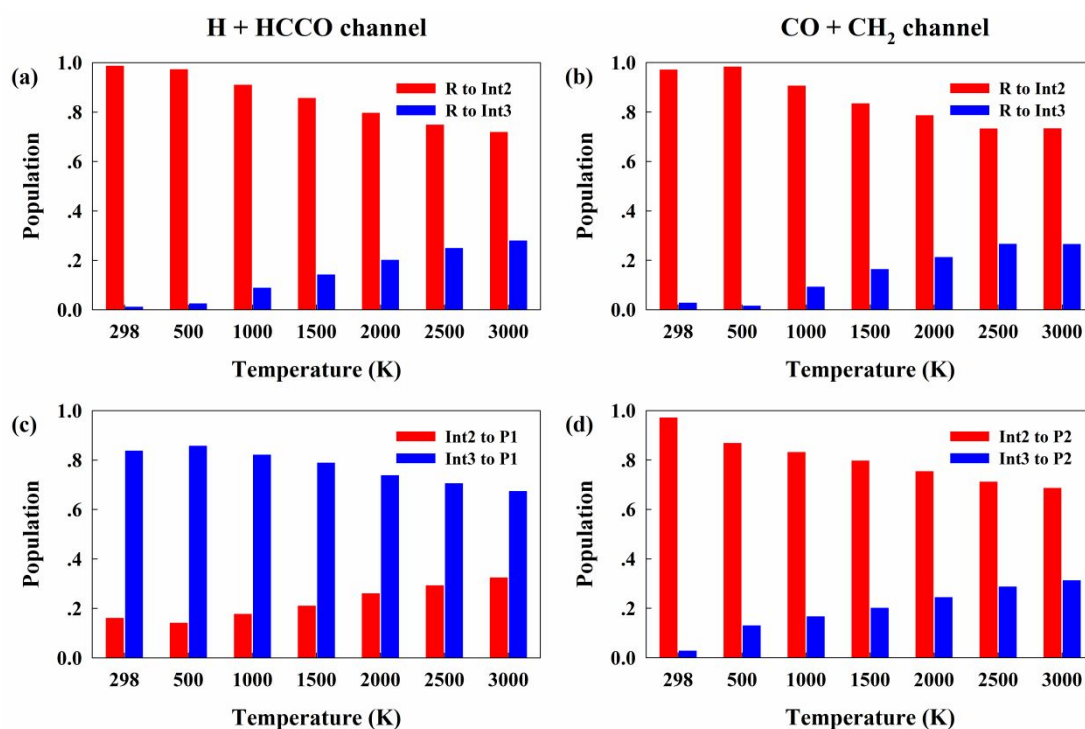


**Fig. 5** Percentages of two key intermediates (Int2 and Int3) for reactive trajectories leading to the H + HCCO channel (left panels) and the CO + CH<sub>2</sub> channel (right panels) at different temperatures. The top two panels are for the initial populations of the two key intermediates after overcoming the rate-limiting transition state (TS1), while the two lower panels are for the final populations of the two key intermediates before exiting to the product channels.

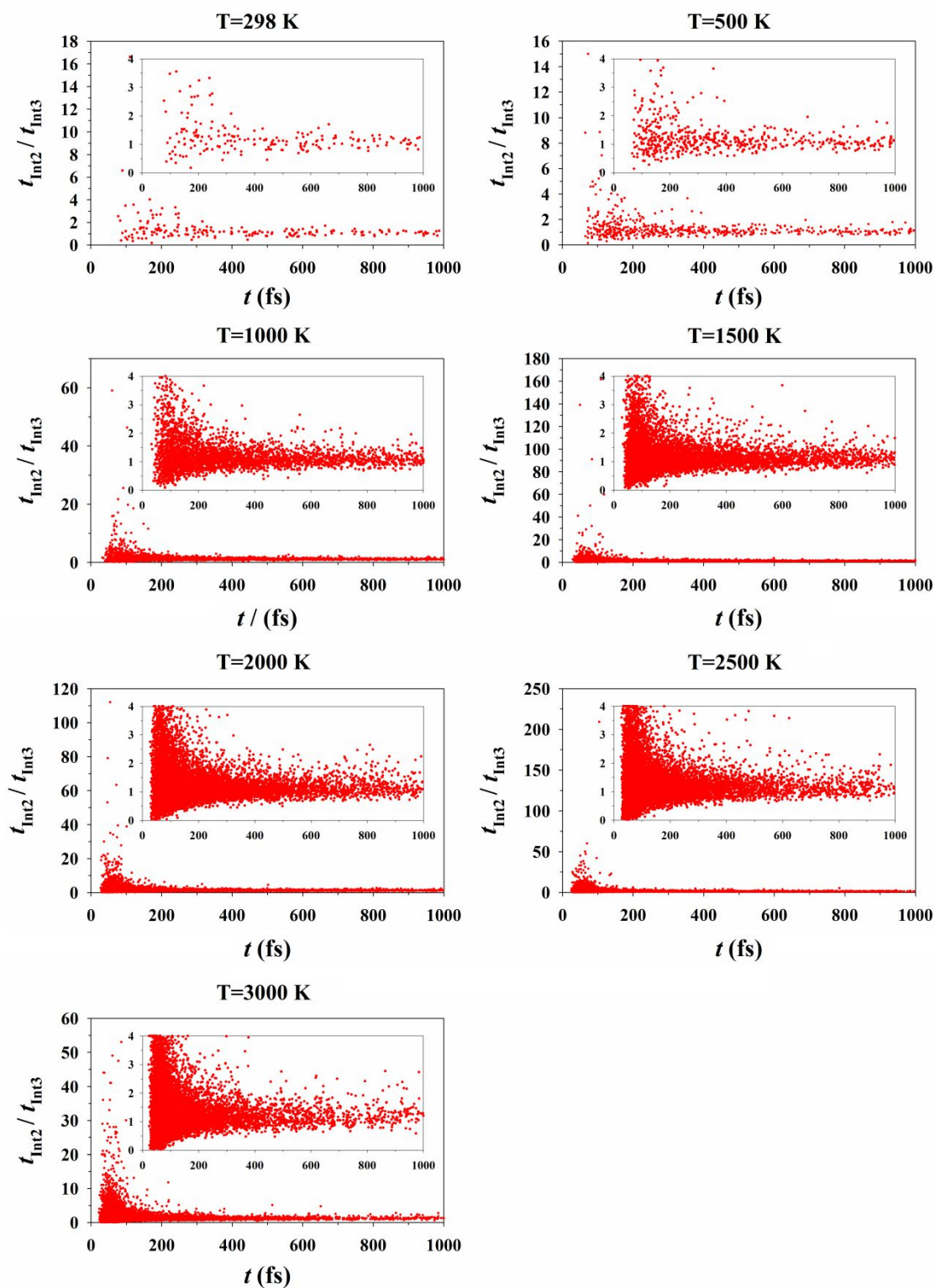


**Fig. 6** Population ratio of the Int2 and Int3 residence times as a function of the total reaction time at several temperatures.

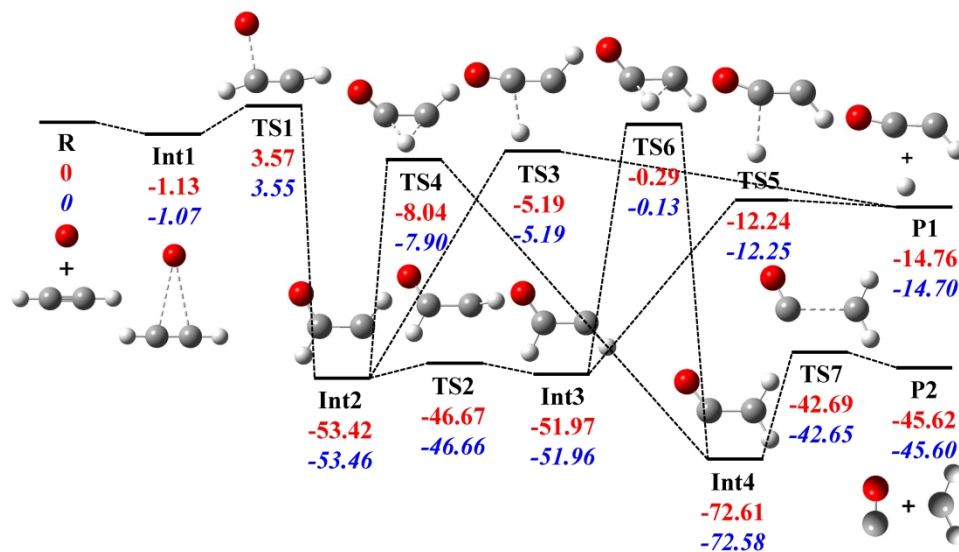


Fig. 1 Schematic illustration of the reaction pathways for the O(3P) + C<sub>2</sub>H<sub>2</sub> reaction. The energies of the stationary points in the fit PES (red) are shown in the figure with the corresponding ab initio values (blue italic). All energies are in kcal/mol relative to the reactant asymptote. The configurations of the reactants (R), products (P1 and P2), reaction complexes (Int1 to Int4), and transition states (TS1 to TS7) are also displayed.

338x190mm (300 x 300 DPI)

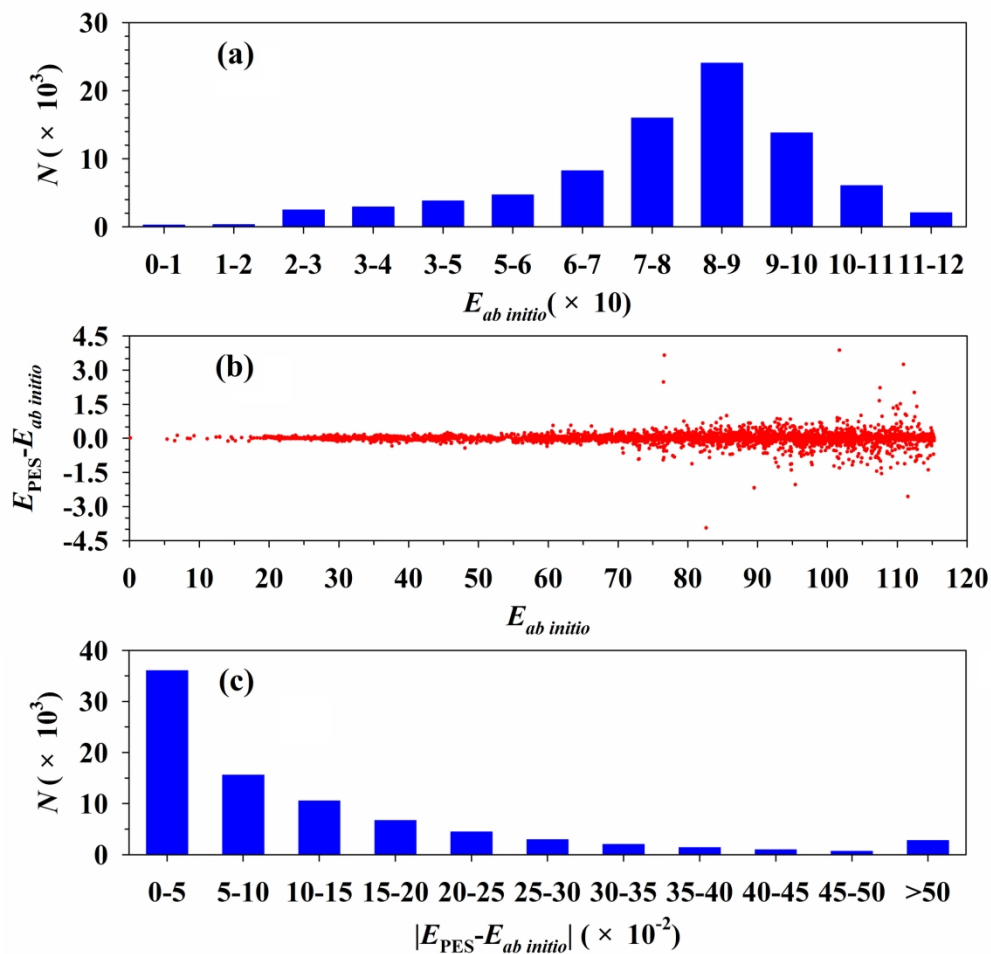


Fig. 2 (a) Distribution of ab initio points for the PIP-NN PES. (b) Fitting errors as a function of the ab initio energy. (c) Distribution of the fitting errors for the selected points. The values of the potential energy are relative to the global minimum, Int4. All energies are in unit of kcal/mol.

196x191mm (300 x 300 DPI)

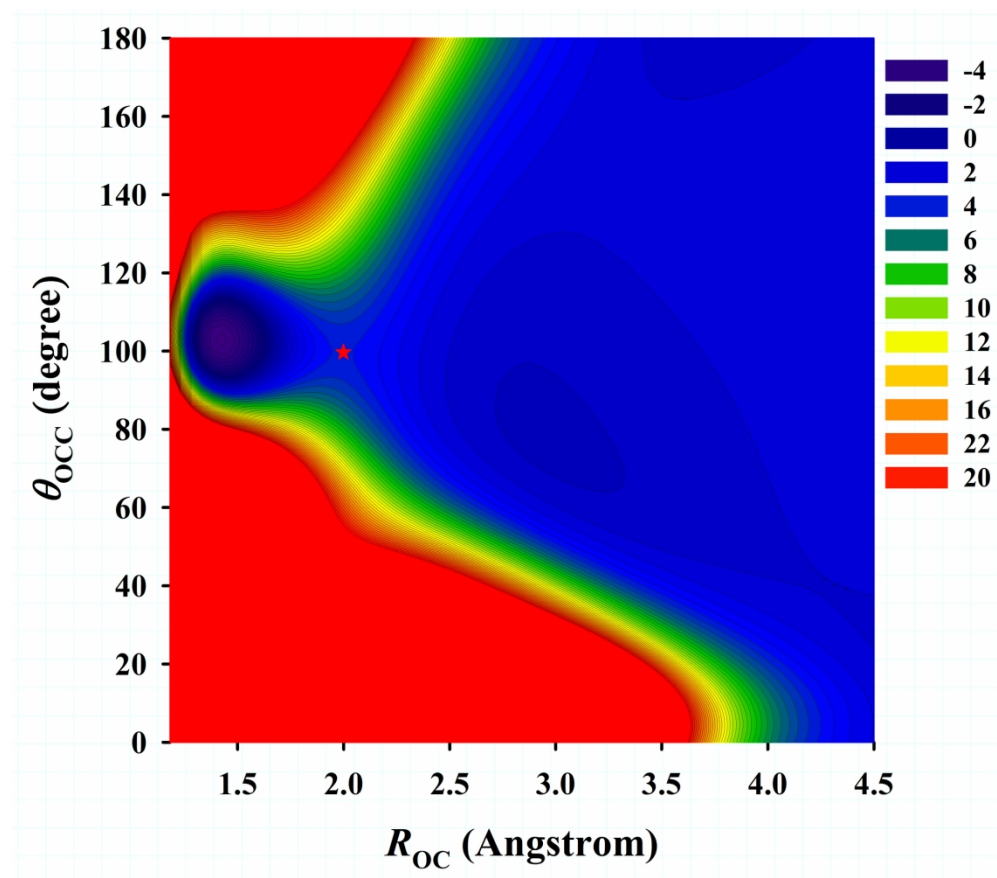


Fig. 3 Contour plots of the OC2H2(3A'') PES as a function of two reactive coordinates,  $R_{OC}$  and  $\theta_{OCC}$ , with all other coordinates constrained at the transition state TS1. The energies are in kcal/mol relative to the O(3P) + C2H2 asymptote with an interval of 0.5 kcal/mol.

177x155mm (300 x 300 DPI)

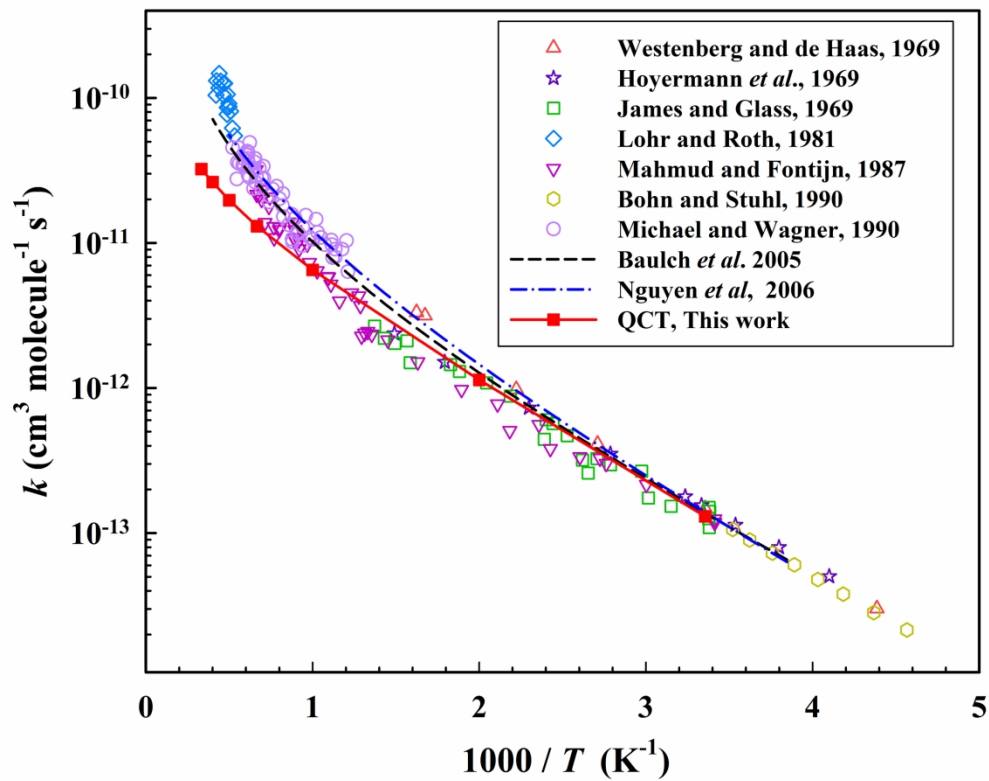


Fig. 4 Arrhenius plot for the O(3P) + C<sub>2</sub>H<sub>2</sub> reaction rate coefficient compared with previous theoretical and experimental results.

199x157mm (300 x 300 DPI)

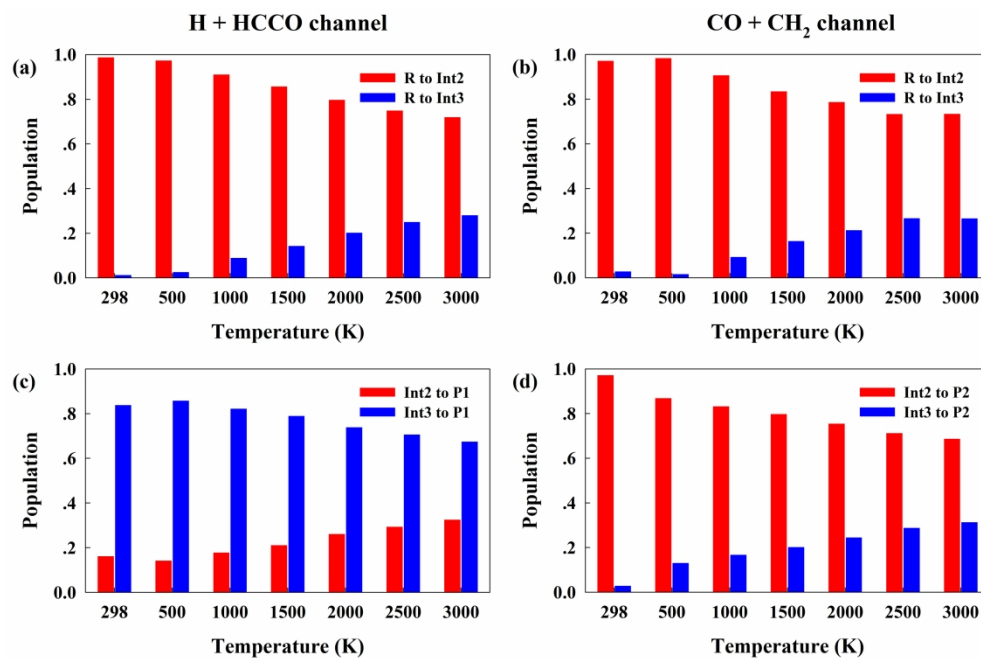


Fig. 5 Percentages of two key intermediates (Int2 and Int3) for reactive trajectories leading to the H + HCCO channel (left panels) and the CO + CH<sub>2</sub> channel (right panels) at different temperatures. The top two panels are for the initial populations of the two key intermediates after overcoming the rate-limiting transition state (TS1), while the two lower panels are for the final populations of the two key intermediates before exiting to the product channels.

268x176mm (300 x 300 DPI)

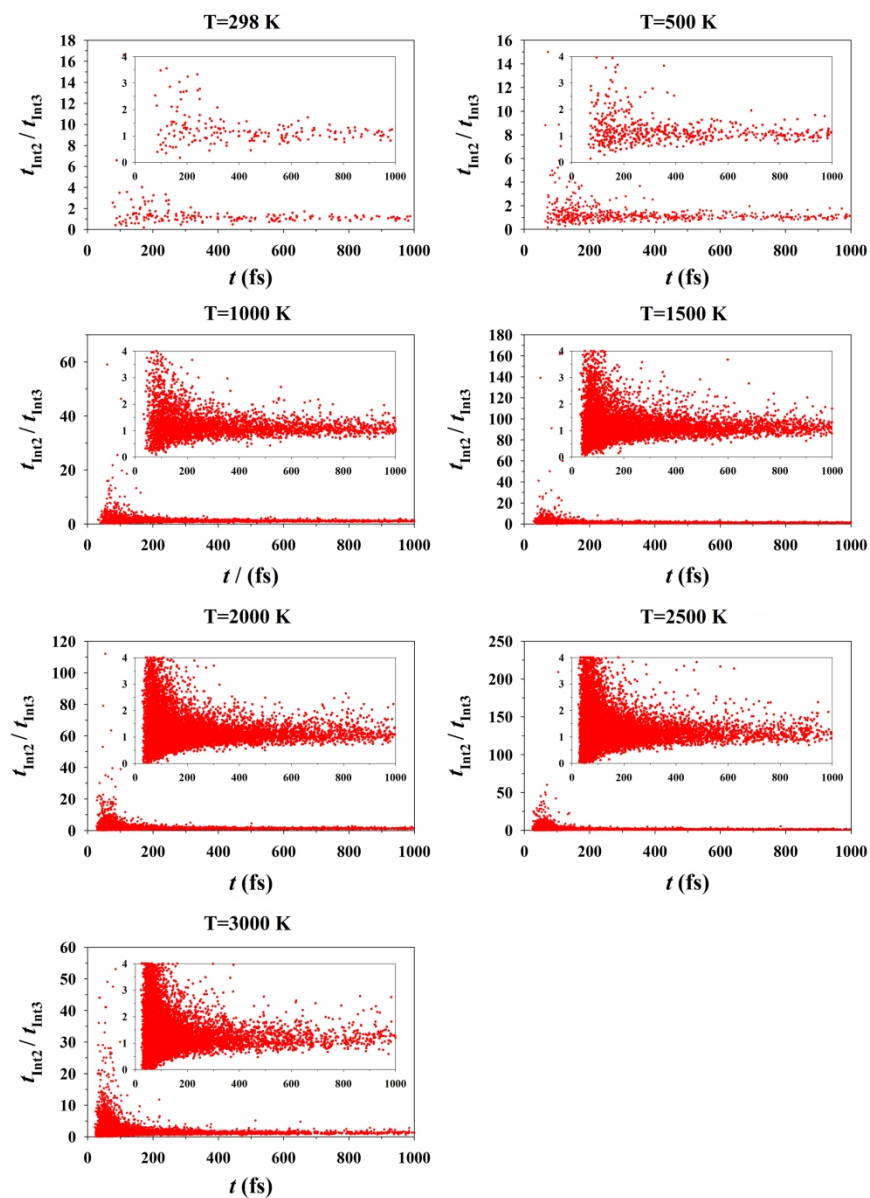


Fig. 6 Population ratio of the Int2 and Int3 residence times as a function of the total reaction time at several temperatures.

206x286mm (300 x 300 DPI)